JACS
JOURNAL OF THE AMERICAN CHEMICAL SOCIETY

ARTICLE

pubs.acs.org/JACS

Comprehensive Studies on an Overall Proton Transfer Cycle of the *ortho*-Green Fluorescent Protein Chromophore

Cheng-Chih Hsieh,[†] Pi-Tai Chou,[*,†] Chun-Wei Shih,[†] Wei-Ti Chuang,[†] Min-Wen Chung,[†] Junghwa Lee,[‡] and Taiha Joo[*,‡]

[†]Department of Chemistry, National Taiwan University, Taipei, 106, Taiwan, R.O.C.

[‡]Department of Chemistry, Pohang University of Science and Technology, Pohang, 790-784, South Korea

ABSTRACT: Initiated by excited-state intramolecular proton transfer (ESIPT) reaction, an overall reaction cycle of 4-(2-hydroxybenzylidene)-1,2-dimethyl-1*H*-imidazol-5(4*H*)-one (*o*-HBDI), an analogue of the core chromophore of the green fluorescent protein (GFP), has been investigated. In contrast to the native GFP core, 4-(4-hydroxybenzylidene)-1,2-dimethyl-1*H*-imidazol-5(4*H*)-one (*p*-HBDI), which requires hydrogen-bonding relay to accomplish proton transfer in vivo, *o*-HBDI possesses a seven-membered-ring intramolecular hydrogen bond and thus provides an ideal system for mimicking an intrinsic proton-transfer reaction. Upon excitation, ESIPT takes place in *o*-HBDI, resulting in a ~600 nm proton-transfer tautomer emission. The *o*-HBDI tautomer emission, resolved by fluorescence upconversion, is comprised of an instantaneous rise to a few hundred femtosecond oscillation in the early relaxation stage. Frequency analysis derived from ultrashort pulse gives two low-frequency vibrations at 115 and 236 cm^{-1}, corresponding to skeletal deformation motions associated with the hydrogen bond. The results further conclude that ESIPT in *o*-HBDI is essentially triggered by low-frequency motions and may be barrierless along the reaction coordinate. Femtosecond UV/vis transient absorption spectra also provide supplementary evidence for the structural evolution during the reaction. In CH_3CN, an instant rise of a 530 nm transient is resolved, which then undergoes 7.8 ps decay, accompanied by the growth of a rather long-lived 580 nm transient species. It is thus concluded that following ESIPT the cis-proton transfer isomer undergoes cis−trans-isomerization. The results of viscosity-dependent dynamics are in favor of the one-bond-flip mechanism, which is in contrast to the volume-conserving isomerization behavior for *cis*-stilbene and *p*-HBDI. Further confirmation is given by the picosecond−femtosecond transient IR absorption spectra, where several new and long-lived IR bands in the range of 1400−1500 cm^{-1} are assigned to the phenyl in-plane breathing motions of the trans-proton transfer tautomer. Monitored by the nanosecond transient absorption, the 580 nm transient undergoes a ~7.7 μs decay constant, accompanied by the growth of a new ~500 nm band. The latter is assigned to a deprotonated tautomer species, which then undergoes the ground-state reverse proton recombination to the original *o*-HBDI in ~50 μs, achieving an overall, reversible proton transfer cycle. This assignment is unambiguously supported by pump−probe laser induced fluorescence studies. On these standpoints, a comparison of photophysical properties among *o*-HBDI, *p*-HBDI, and wild-type GFP is discussed in detail.

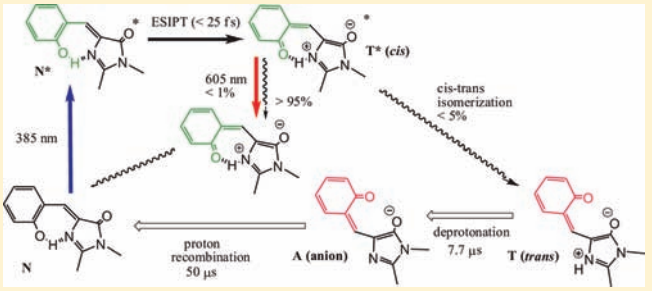

1. INTRODUCTION

Green fluorescence protein (GFP), which serves as an energy acceptor and emitter for bioluminescence in the sea pansy *Renilla reniformis* and the jellyfish *Aequorea victoria*, has been the subject of a great deal of interest because of its ubiquitous applications in molecular biology.[1] GFP takes advantage of the presence of 4-(4-hydroxybenzylidene)-1,2-dimethyl-1*H*-imidazol-5(4*H*)-one, which has been intensively investigated as its dimethyl derivative 4-(4-hydroxybenzylidene)-1,2-dimethyl-1*H*-imidazol-5(4*H*)-one (*p*-HBDI) (Scheme 1). The GFP core chromophore is anchored on the protein both covalently and via a hydrogen-bonding network linking two ends of the chromophore, including the hydroxyl of Tyr66, a water molecule, the side-chain hydroxyl of Ser205, the carboxylate group of Glu222, and the side-chain hydroxyl group of Ser65.[2] The excited-state proton transfer (ESPT)[3] thus takes place via the proton relay of water molecules and the amino acid residues to a remote residue such as Glu222,[2−4] resulting in a very effective and intense anion fluorescence.

In terms of chemistry, most of the research has focused on the chemical modification of *p*-HBDI[5] analogues at the C(1) position (Scheme 1), such that the emission color can be fine-tuned via the substituent effect.[6] Nevertheless, studies reveal a sharp cut off between the properties of wild type GFP (or certain GFP mutants) and the synthetic core chromophore *p*-HBDI or its derivatives. In terms of photophysical properties, the fluorescence of the protein-free *p*-HBDI in fluid solvents is very dim

Received: September 9, 2010
Published: February 16, 2011

dx.doi.org/10.1021/ja107945m | *J. Am. Chem. Soc.* 2011, 133, 2932–2943

Scheme 1. The Molecular Structure of *p*-HBDI, *o*-HBDI, and *o*-MBDI

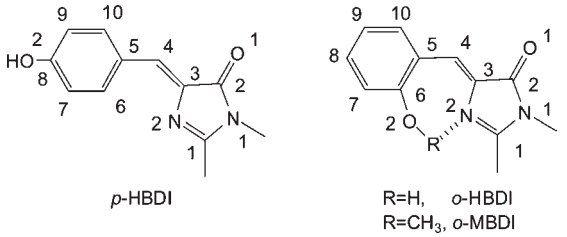

($<10^{-3}$ at 298 K)[5c] and shows strong temperature dependence. During the past decades, the excited-state relaxation dynamics of free *p*-HBDI chromophore has been investigated by various spectroscopic techniques, such as time-resolved fluorescence upconversion,[7] UV/vis transient absorption,[8] and UV pump/IR probe spectroscopy.[9] The lifetime of *p*-HBDI was determined to be ~1 ps in solution phase without the occurrence of ESPT. Similar to the stilbene-like isomerization[10] around the exocyclic C═C double bond, it has been proposed that the deactivation pathways of *p*-HBDI are mainly governed by the internal conversion to the ground state, induced by the cis−trans-isomerization.[11] This process causes the molecular relaxation on the excited-state potential energy surface funneling toward a minimum of a shallow potential energy surface that possesses a twisted/perpendicular geometry (cf. the planar structure). As a result, the close approach or even conical intersection between ground and excited states potential energy surface gives rise to a rapid internal conversion process.[10] Supported by the quantum chemical calculations, Weber et al.[12] proposed that the isomerization incorporated the rotation along the bridging C═C−C bonds, for which one-bond flip and concerted twist, i.e. the hula type of twist (vide infra), were both favorable. Mandal et al.[7c] further concluded that the mechanism was more likely due to the incorporation of rotation along a concerted twist of the bridging C═C−C bonds, i.e. a hula-twist[13] type of motion, based on the solvent-viscosity-independent relaxation dynamics.[7] More recently, via probing a series of *p*-HBDI analogues, an additional internal nucleophile mechanism has also been proposed to mediate their photophysical properties.[14] In yet another approach, the structural changes of the core chromophore in wild-type GFP have also been studied.[15] In stark contrast, ESPT takes place in wild-type GFP, whereas the isomerization relaxations would be highly prohibited due to the rigid H-bonding environment of the core moiety inside the protein, giving much different aspects in photophysical behavior regarding the protein-free *p*-HBDI core.

Recently, we have strategically designed and synthesized a structural isomer of the core chromophore (*p*-HBDI), namely, 4-(2-hydroxybenzylidene)-1,2-dimethyl-1*H*-imidazol-5(4*H*)-one (*o*-HBDI)[16] (Scheme 1). *o*-HBDI possesses a seven-membered-ring hydrogen bond, from which the excited-state intramolecular proton transfer (ESIPT) takes place free from the assistance of guest molecules (solvents, self-dimerization, etc.), giving rise to a large Stokes shifted proton-transfer tautomer emission of ~600 nm in solution. ESIPT also takes place in the solid film, resulting in a unique ~595 nm tautomer emission. The result is in sharp contrast to the prohibition of ESPT as well as extremely weak (normal) emission for protein-free *p*-HBDI. Conversely, the results are reminiscent of that of the hydrogen-bonded network induced proton transfer reaction for *p*-HBDI in wild GFP.

Taking advantage of the intrinsic ESIPT reaction, we herein report comprehensive studies of an overall proton transfer reaction cycle of *o*-HBDI. The *o*-HBDI proton-transfer tautomer emission is first resolved by fluorescence up-conversion with a time resolution of <30 fs in an attempt to extract the reaction pattern. We then made further attempts to probe the structural evolution of *o*-HBDI by using time-resolved UV-vis and mid-infrared spectroscopy. This, in combination with steady-state and nanomicrosecond pump−probe transient absorption and two-step laser-induced fluorescence, provides in-depth insight into the associated reaction dynamics during an ESIPT → cis−trans-isomerization → deprotonation → ground-state reverse proton transfer cycle. The results thus serve as a paradigm for fair comparison with respect to the protein-free *p*-HBDI core and wild-type GFP.

2. EXPERIMENTAL SECTION

2.1. Synthesis. The *o*-GFP core chromophore analogues 4-(2-hydroxybenzylidene)-1,2-dimethyl-1*H*-imidazol-5(4*H*)-one (*o*-HBDI) and its methylated compound 4-(2-methoxybenzylidene)-1,2-dimethyl-1*H*-imidazol-5(4*H*)-one (*o*-MBDI) were prepared according to a synthetic route in our previous report.[16] Besides acetonitrile-d_3 (Cambridge Isotope Laboratories, Inc.), other solvents were purchased from Merck and distilled from appropriate drying agents prior to use. Commercially available reagents were used without further purification unless otherwise stated. All reactions were monitored by TLC with Macherey-Nagel precoated Glassic sheets (0.20 mm with fluorescent indicator UV254). Compounds were visualized with UV light at 254 and 365 nm. Flash column chromatography was carried out using silica gel from Merck (230−400 mesh).

2.2. Steady-State and Femtosecond Time-Resolved Fluorescence Spectroscopy. Steady-state UV/vis absorption and emission spectra were recorded by a Hitachi (U-3310) spectrophotometer and an Edinburgh (FS920) fluorimeter, respectively. Infrared spectra were recorded on a Nicolet Magna II 550 FTIR apparatus with automatic background subtraction by using two BaF_2 plates as the sample cell. The setup of femtosecond dynamical measurements has been elaborated in detail in our previous report.[17] Briefly, the original light source was based on a femtosecond Ti-sapphire oscillator (80 MHz, Spectra Physics). The fundamental train of pulses (700−960 nm) was used to produce the second harmonics (SH, 350−480 nm) for the excitation light source. A polarizer was placed in the emission path to ensure that the polarization of the fluorescence was set at the magic angle (54.7°) with respect to that of the excitation light to eliminate the fluorescence anisotropy. The up-converted signal was separated by a single monochromator (CDP2022, CDP Systems Corp.) and detected via a photon-counting PMT (R1527P, Hamamatsu). The cross correlation between SH and the fundamental had a full width at half-maximum (fwhm) of ~180 fs, which was chosen as a response function of the system.

To resolve the initial ultrafast dynamics, including the coherent nuclear motion, time-resolved fluorescence was also recorded at higher time resolution. The light source was a home-built cavity-dumped Ti:sapphire laser, generating 22 fs pulses at 800 nm. Pump pulses at 400 nm were produced by the second harmonic generation in a 100 μm thick β-barium borate (BBO) crystal, and the remaining fundamental served as gate pulses. In order to prevent photodamage, the energy and repetition rate of the pump pulses with spot size 20 μm in diameter were reduced to 1 nJ and 380 kHz, respectively. The time-resolved fluorescence apparatus, which delivers sub-50 fs resolution by utilizing a noncollinear sum

frequency generation (SFG) scheme, has been described in detail elsewhere.[18] The SFG was carried out in a 300 μm thick BBO crystal with an external angle of 20°. Cross correlation between the scattered pump and the gate pulses was ~35 fs, which allowed the detection of nuclear wave packet motions as high as 500 cm^{-1}.

2.3. Femtosecond UV/Vis Transient Absorption Measurements. The femtosecond UV/vis transient absorption measurements were also performed according to the previous reports.[19] Briefly, a femtosecond Ti:sapphire amplifier (Spitfire Pro, Spectra Physics) was used as the light source. The output of the system consists of pulses of 800 nm, 1 W, 120 fs (fwhm) at a repetition rate of 1 kHz. The pump−probe spectroscopic setup is based on an ExciPro spectrometer (CDP Systems Corp.). The laser amplifier output is first split (50%) into two beams, in which the pump is converted to designated excitation wavelengths by coupling it into a second-harmonic generator (for 400 nm excitation). The probe is focused on a 1 mm thick sapphire plate to generate a white light continuum (450−1000 nm). The pump beam is then passed through a computer-controlled optical chopper and focused (3 mm) on the sample cell. The sample cell is a 1 mm optical path quartz cylindrical cell placed in a variable speed rotating holder. After passing through the sample cell, the white continuum is coupled into a 100 μm optical fiber connected to a diode array. Typically, time-resolved absorption spectra were acquired, averaging over 200 excitation pulses at any delay time. The effective time resolution of the ultrafast spectrometer is determined to be about 200 fs.

2.4. Femtosecond UV Pump/Mid-IR Probe Spectroscopy. Femtosecond infrared spectroscopy is performed by initiating the ESIPT reaction with a UV pump at 400 nm to excite *o*-HBDI to the S_1 state and probe from 1730 to 1300 cm^{-1}. The experimental setup of UV-pump/mid-IR probe spectroscopy was similar to that reported by Elsaesser and co-workers.[20] Excitation was performed using near-UV pulses, which were generated by the second-harmonic generation (β-BaB_2O_4 crystal, 0.2 mm thickness) of the fundamental of the 1 kHz Ti:sapphire amplifier (Spitfire Pro, Spectra Physics). The mid-infrared pulses were generated using a traveling-wave optical parametric amplifier of the white-light continuum (TOPAS-C, Spectra Physics), followed by difference frequency mixing of the signal and idler in a $AgGsS_2$ crystal. The femtosecond UV pump/mid-IR probe spectroscopic setup was based on a TAPPIR spectrometer (CDP Systems Corp.) with slight modification of optics and the optical light path to improve both sensitivity and stability. Probe and reference pulses were derived using reflections from a BaF_2 wedge and focused onto the sample with a 200 μm optical path length BaF_2 cylindrical cell placed in a variable-speed rotating holder. Subsequently, the probe and reference pulses were dispersed in a monochromator (Jobin Yvon, HR320), and complete spectra were recorded simultaneously for each shot using two liquid nitrogen cooled HgCdTe photodiodes as the reference and sample, respectively. A synchronized chopper was then applied for pump light modulation. The 1:1 chopping ratio, in which one pump pulse pass causes the next one to be blocked, gives an optimum S/N ratio and shortest data acquisition time. The effective time resolution of the ultrafast spectrometer, that is, the rise time of an "instantaneous" signal, is about 250 fs.

2.5. Nanosecond Time-Resolved Spectroscopy. Nanosecond transient absorption was recorded with a laser flash photolysis system (Edinburgh LP920), in which the third harmonic (355 nm, fwhm ~15 ns) of a Nd:YAG laser (Continuum Surelite) and a white light square pulse were used as the pump and probe beams, respectively. These two pulses were crossed at a 90° angle with an overlapping distance of 10 mm. The temporal resolution was limited by an excitation pulse duration of approximately 15 ns. A sample solution of ~6 mL was used in the nanosecond transient absorption experiments. A detailed description of the setup for the nanosecond transient absorption and two-step laser induced fluorescence (TSLIF) has been reported previously.[21] Briefly, the second harmonic (400 nm, fwhm ~20 ns) of a Nd:YAG pumped Ti:sapphire laser (LT-2211, LOTIS TII) was used as the excitation pulse, and the second harmonic (532 nm, fwhm ~15 ns) of the flash lamp pumped, Q-switched Nd:YAG laser (Continuum Surelite) was applied as the probe pulse. Both pump and probe pulses were skimmed to a rectangular shape of 2.5 mm × 4.0 mm and projected at a 0° angle across the sample cell in order to achieve maximum overlap. The time delay between the pump and the probe pulses was monitored by a programmable delay pulse generator (SRS model DG-535). The fluorescence was then detected by an optical spectrum analyzer, consisting of an intensified charge-coupled device (ICCD) with detector control (PI-MAX, Princeton Instruments) in conjunction with a monochromator (SP2300i, Acton). The gate channel of the ICCD was open at 50 ns and synchronized with the firing time of the probe pulse. For all time-resolved measurements, steady-state absorption spectra were recorded before and after experiments to ensure negligible decomposition during data acquisition.

2.6. Theoretical Approach. Ground-state and the lowest singlet excited-state (S_1) geometries were optimized by the density functional theory (DFT) with B3LYP hybrid functional[22] and CIS theory,[23] respectively. The 6-31G(d) basis sets were employed for all atoms.[24] The simulated IR spectra (frequencies and intensities) were deduced on the basis of the optimized structures using a bandwidth of 20 cm^{-1} in combination with an integral equation formalism-polarizable continuum model (in acetonitrile), IEF-PCM.[25] All calculations were carried out using the Gaussian 03 program.[26]

3. RESULTS

3.1. Steady-State UV/Vis Absorption/Emission and Time-Resolved Fluorescence. Figure 1 shows the steady-state absorption and emission spectra of *o*-HBDI in various aprotic solvents. Pertinent photophysical properties of *o*-HBDI are also listed in Table 1. Both absorption and emission spectra show only slight solvent-polarity dependence. For example, the lowest lying absorption maxima are located at 385 and 383 nm, while the emission peaks are resolved at 605 and 602 nm in cyclohexane and acetonitrile, respectively. The absence of normal form emission and the appearance of a large Stokes shift of ~9000 cm^{-1} between absorption and emission spectra unambiguously support the occurrence of the ultrafast ESIPT reaction of *o*-HBDI in all solvents applied.

The dynamics of ESIPT for *o*-HBDI were then probed by monitoring the proton-transfer tautomer emission in various aprotic solvents. In this fluorescence up-conversion measurement, *o*-HBDI was excited at the region of 390−410 nm, the energy of which is near the onset of $S_0 \rightarrow S_1$ transition (Figure 1). The time-resolved tautomer emissions monitored at the peak in various solvents at the time resolution of ~180 fs are depicted in Figure 2. In all solvents, a general trend is observed in that the time trace can be convoluted by the sum of a system-response-limited rise component (<180 fs) and two exponential decays (see Table 1). The fast decay time constants are determined to be <1.5 ps, while the longer decay component reveals significant solvent dependence (vide infra). The <180 fs rise of the tautomer emission affirms ultrafast ESIPT for *o*-HBDI in all solvents applied. Moreover, due to the exergonic type of ESIPT, it is plausible that the <1.5 ps fast decay component originates from the vibronic relaxation of the tautomer initially prepared via ESIPT reaching the thermal equilibrium. The population decay (τ_2) reveals significant solvent dependence (see Figure 2 and Table 1), for which the lifetimes are determined to be 8 ps in acetonitrile ($\eta \sim 0.34$ cP), 32 ps in cyclohexane (0.93 cP), 49 ps

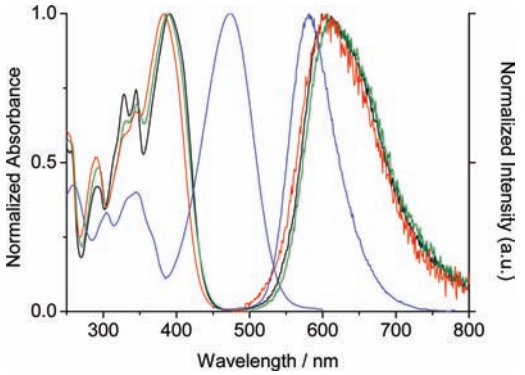

Figure 1. Steady-state absorption and emission spectra of *o*-HBDI in cyclohexane (black), dichloromethane (green), and acetonitrile (red). The absorption and emission of deprotonated *o*-HBDI in acetonitrile saturated with NaOH (blue line).

Table 1. Decay Parameters of *o*-HBDI in Various Solvents

solvents	η/cP	ε	τ_1[a]/ps	τ_2/ps	quantum yield (Φs)
CH_3CN	0.34	37.5	0.4 (0.27)	7.8	1.5×10^{-3}
THF	0.46	7.52	0.3 (0.20)	15.2	2.1×10^{-3}
CH_2Cl_2	0.42	9.08	0.3 (0.23)	16.6	2.2×10^{-3}
cyclohexane	0.93	2.02	0.1 (0.12)	31.9	3.1×10^{-3}
toluene	0.57	2.38	0.2 (0.07)	37.8	3.3×10^{-3}
dodecane	1.46	2.00	0.8 (0.03)	48.8	5.7×10^{-3}
1-octadecene	3.58	2.25	1.3 (0.02)	70.9	6.2×10^{-3}

[a] .The fast component has been fitted with an accuracy of ±40%. The weights of the fast component are shown in parentheses (normalized to 1).

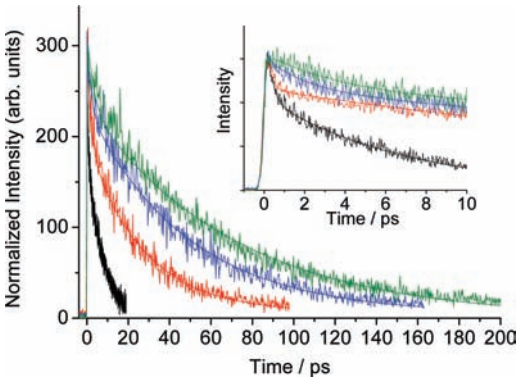

Figure 2. The femtosecond time-resolved fluorescence spectra of *o*-HBDI monitored at 600 nm in acetonitrile (black), cyclohexane (red), dodecane (blue), and 1-octadecene (green). (Inset) The early relaxation dynamics of *o*-HBDI in acetonitrile (black), cyclohexane (red), dodecane (blue), and 1-octadecene (green).

in dodecane (1.46 cP), and 71 ps in 1-octadecane (3.58 cP), while it is as long as 1.7 ns in solid film at room temperature. The fluorescence lifetimes correlate well with the associated steady-state quantum yields, which increase from 1.5×10^{-3} in acetonitrile to 6.2×10^{-3} in 1-octadecene (for details, see Table 1). In solid film, the tautomer emission yield is as high as 0.40.[16] Apparently, both the fluorescence lifetime and the

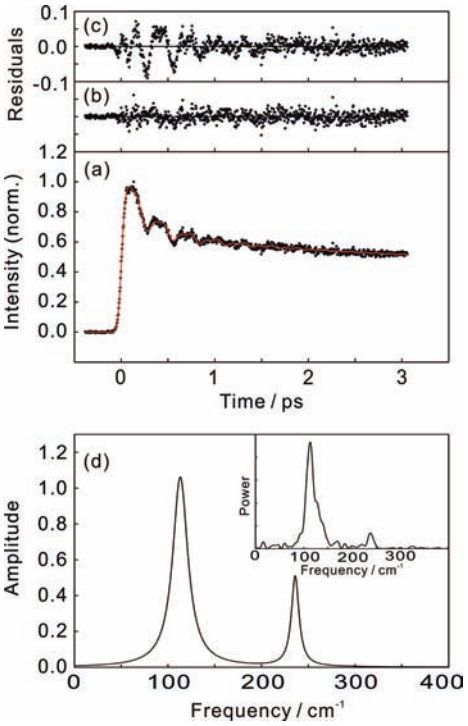

Figure 3. (a) Ultrashort pulse time-resolved fluorescence signal of *o*-HBDI in cyclohexane monitored at cis-proton transfer tautomer emission at 600 nm. The red line is the nonlinear least-squares fit to a sum of three exponentials and two damped sinusoids as described in the text. Residuals for the fit are shown in part b. Residuals for the exponential fit not including the damped sinusoids are also shown in part c. (d) Spectra of the oscillatory components obtained by the linear prediction singular value decomposition (LPSVD) method. (Inset) Fourier transform power spectrum of the residuals shown in part c. Note that relative height of the peak around 240 cm^{-1} in the FT power spectrum is smaller than that in the LPSVD spectrum because of the quadratic nature of FT power spectrum.

quantum yield of *o*-HBDI show a lack of solvent-polarity dependence but a strong correlation with respect to the solvent viscosity.

To gain in-depth insight into the mechanism of ESIPT, time-resolved fluorescence with much higher time-resolution (~25 fs) was also obtained.[18] Figure 3a shows the time-resolved fluorescence of *o*-HBDI monitored at the proton-transfer tautomer emission (~600 nm) in cyclohexane. The signal shows an instant rise (<25 fs), indicating that the ESIPT in *o*-HBDI is perhaps barrierless. In addition to the 1.5 and 37 ps decay components, which correspond to the τ_1 and τ_2 components, respectively, in Table 1, a much faster 220 fs decay component was also observed. A decay with the similar time scale has been reported for other ESIPT molecules,[18c] although its origin is controversial; intramolecular vibrational redistribution (IVR),[27] vibronic relaxation,[28] and internal conversion from the initially formed S_2 (L_a) state to close lying S_1 (L_b)[17] have been proposed to explain its origin. The highly time-resolved fluorescence signal of the tautomer emission also reveals oscillations due to the vibrational wave packet motion in the excited tautomer potential surface. The vibrational coherence in the product (tautomer) is a result of the ultrafast proton transfer, which is impulsive for the low-frequency vibrations. Linear prediction singular value decomposition (LPSVD) analysis resolved two oscillation

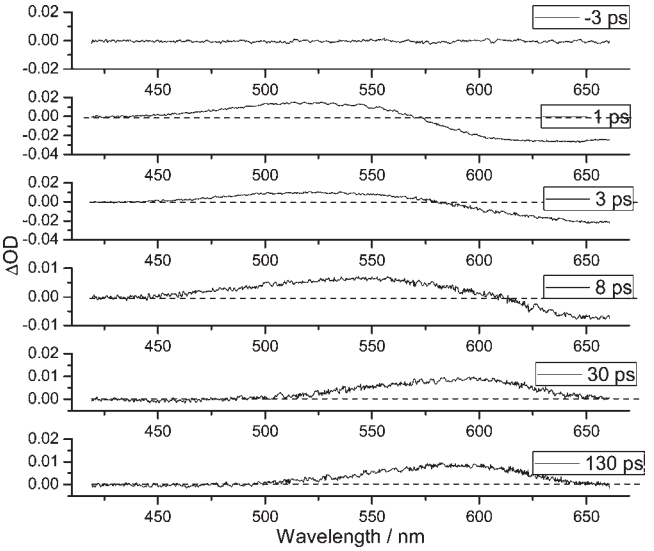

Figure 4. The femtosecond UV/vis transient absorption spectra of *o*-HBDI in CH_3CN upon excitation at 400 nm.

frequencies at 115 and 236 cm^{-1}. Quantum mechanical calculation showed that they are the two lowest frequency in-plane skeletal vibrational modes that modulate the OH distance strongly. This directly indicates that the emission band around 600 nm is indeed due to the tautomer product and that the reaction is fast enough to be impulsive for the 236 cm^{-1} vibrational mode, for example; that is, the reaction must be faster than roughly half of the vibrational period (~70 fs). This, in combination with the lack of deuterium isotope dependence in the rise dynamics, leads us to conclude that ESIPT in *o*-HBDI is essentially triggered by low-frequency motions and may be barrierless along the reaction coordinate. The low-frequency vibrational modes are plausibly associated with skeletal deformation involving hydrogen bonds (O−N distance or O−H···N angle, vide infra).

3.2. Femtosecond−Picosecond UV/Vis Transient Absorption. We then performed femtosecond−picosecond UV/vis transient absorption experiments in an aim to gain complementary support for the reaction dynamics. Serendipitously, the study provides new, previously unrecognized insight (cf. time-resolved fluorescence) into the excited-state relaxation dynamics after ESIPT. Figure 4 depicts the transient absorption spectra of *o*-HBDI in CH_3CN acquired at pump−probe delay times ranging from 0.2 to 130 ps. Following the photoexcitation, simultaneously, there appears a transient absorption band at 530 nm and a stimulated emission signal maximized at 615 nm. The stimulated emission at 615 nm matches the steady-state 605 nm proton-transfer emission of *o*-HBDI in CH_3CN. As the time elapses, the 530 nm transient gradually disappears, accompanied by the growth of a red-shifted signal toward 550 nm at, for example, 8 ps, which further shifts to 580 nm at, for example, 30 ps and then remains unchanged up to the longest delay of 130 ps, such that the current system can still maintain precision in spatial overlapping between pump and probe pulses. Because the τ_f of proton-transfer emission is 7.8 ps in CH_3CN, the ≫30 ps transient absorption with lack of corresponding fluorescence could not be associated with the excited-state but rather with the ground-state phenomenon. Similarly, the long-lived transient absorption signal at ~570 nm can be detected in other polar solvents, such as tetrahydrofuran and toluene, but is absent in nonpolar solvents such as cyclohexane. Details will be elaborated in the Discussion section.

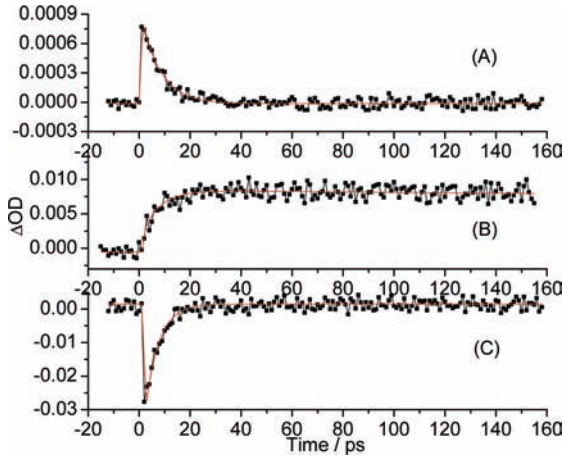

Figure 5. The relaxation dynamics of femtosecond UV/vis transient absorption spectra of *o*-HBDI in CH_3CN monitored at (A) 470 nm, (B) 580 nm, and (C) 640 nm, respectively.

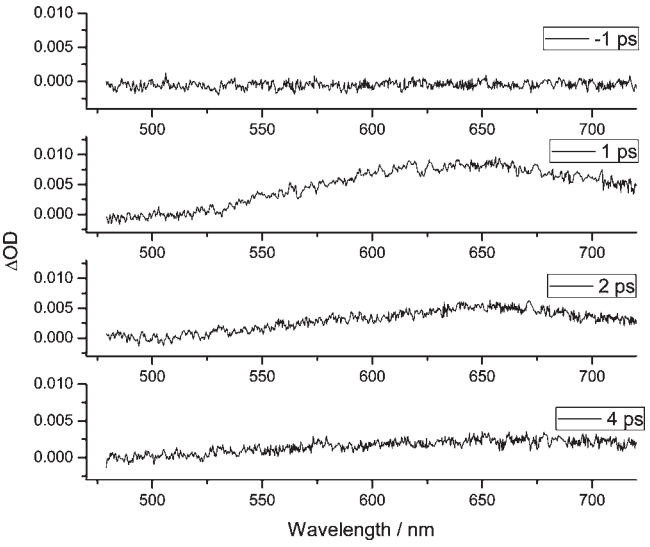

Figure 6. The femtosecond UV/vis transient absorption spectra of *o*-MBDI in CH_3CN upon excitation at 400 nm.

The temporal behavior of the *o*-HBDI transient absorption at several characteristic wavelengths, such as 470, 580, and 640 nm, is plotted in Figure 5. The transient absorption signal at 470 nm can be well-fitted by a single exponential decay of 7.2 ps, which correlates well with the single exponential decay of 6.8 ps of the stimulated emission signal monitored at 640 nm. Moreover, upon monitoring at the long-lived transient absorption band of ~580 nm, the kinetic data shows a 7.3 ps rise component, followed by a much longer decay time constant that cannot be determined with the current subpicosecond transient system (vide supra).

As a control experiment for the above experiments regarding *o*-HBDI, the UV/vis transient absorption spectra of methylated analogue, *o*-MBDI, in CH_3CN has also been investigated. Note that ESIPT is prohibited for *o*-MBDI due to the lack of a

dx.doi.org/10.1021/ja107945m |*J. Am. Chem. Soc.* 2011, 133, 2932–2943

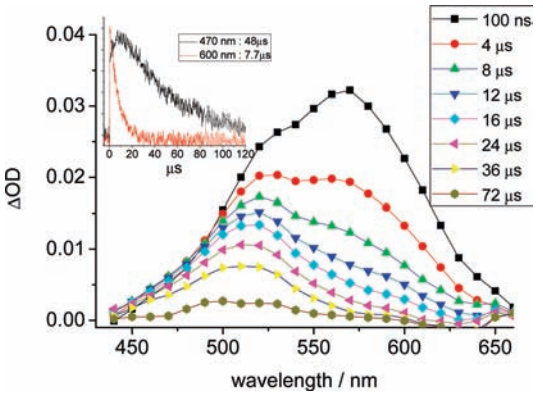

Figure 7. The nanosecond UV/vis transient absorption spectra of *o*-HBDI in CH_3CN. (Inset) The time-dependent signal monitored at 470 and 600 nm, respectively.

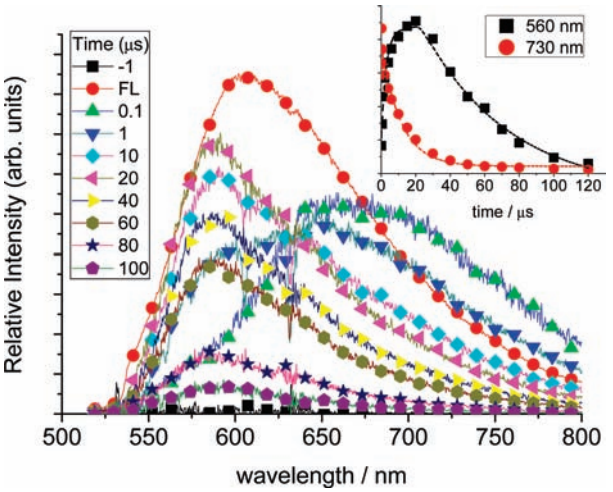

Figure 8. The TSLIF spectra of *o*-HBDI in CH_3CN. (Inset) The time-dependent intensity monitored at 560 and 730 nm, respectively. Note that FL denotes the normalized steady-state emission spectrum of *o*-HBDI in CH_3CN.

hydroxyl proton. As shown in Figure 6, *o*-MBDI reveals only one transient absorption band maximized at ~650 nm, the spectral feature of which is completely different from that of *o*-HBDI. This 650 nm absorption band decreases rapidly, and the decay dynamics can be deconvoluted by a single exponential decay with the time constant 2.1 ps, which is very similar to the fluorescence lifetime.[16] In view of the quite different transient spectral feature, as well as the associated decay dynamics between *o*-MBDI and *p*-HBDI, the occurrence of ESIPT, followed by a subsequent, for example, isomerization reaction is evident.

3.3. Nanosecond−Microsecond Time-Resolved Experiment. To further resolve the unexpectedly long decay component, we then in addition performed a nanosecond transient absorption together with two-step laser-induced fluorescence (TSLIF) measurements. The results shown in Figure 7 clearly reveal that *o*-HBDI exhibits a strong absorption band maximized at ~575 nm after a delay of the probe pulse of, for example, 100 ns. The spectral feature of this transient absorption signal, within experimental error, is identical to the long-lived signal (~580 nm) observed at a delay time of 130 ps in the sub-picosecond measurement (vide supra). Interestingly, however, the 575 nm absorption band then gradually disappears, accompanied by the growth of a new transient absorption maximized at ~500 nm (see Figure 7). Upon monitoring at 600 nm, the lifetime is fitted to be 7.7 μs. We further monitored the blue region (~470 nm) of the 500 nm absorption to suppress interference from the 575 nm transient absorption band. As a result, a decay time constant of 50 μs was determined for the 500 nm band (see the inset of Figure 7). Also, the rise component was resolved to be 7.5 μs at 470 nm, although overlap with respect to the 575 nm band is still unavoidable, as evidenced by the ~50% instant (see Figure 7, system response limit of ~10 ns) rise component.

The identical decay (575 nm band) and rise (500 nm band) time constant indicate a processor−successor type of relationship between these two long-lived transient absorption bands. To provide further insight into these transient species, the pump (400 nm)−probe (532 nm) two-step laser induced fluorescence (TSLIF) spectra are shown in Figure 8. At the pump−probe delay time of 20−100 ns, the results reveal only one emission band maximized at ~670 nm. The intensity of the 670 nm emission band then decreases upon increasing the pump−probe delay time from 100 ns to 80 μs, accompanied by the growth of a 580 nm emission. A plot of the TSLIF emission intensity at the red edge, for example, 730 nm, as a function of pump−probe delay time reveals single exponential decay kinetics, and the lifetime is determined to be 7.8 μs, while monitoring at 560 nm emission intensity resolves a 7.9 μs rise and a decay time constant of 53 μs. These time constants are all in good agreement with the dynamics obtained from those of nanosecond−microsecond transient absorption measurement.

3.4. Time-Resolved Structural Analyses. The time-resolved structural information should provide direct support of ESIPT and any following reaction processes. We herein employed the femtosecond time-resolved UV-pump/mid-IR probe spectroscopy to investigate the corresponding vibrational changes. The present study focuses on the region of the vibrational spectra 1300−1730 cm^{-1} that is expected to undergo appreciable changes due to the characteristic reaction pattern, such as enol−keto and/or cis−trans-isomerization, etc. (vide infra). For fair comparison, Figure 9a shows the ground-state vibrational spectra of *o*-HBDI in CD_3CN measured by FTIR. The structure and vibrational spectra of *o*-HBDI in the enol normal form, which exists predominantly in the ground state, were also calculated by using the B3LYP/6-31G(d) level of theory implemented in Gaussian 03. The assignments of major vibrational peaks in the region of 1300−2000 cm^{-1} are listed in Table 2. Good agreement between experimental and theoretical approaches allows the assignment of essentially all the absorption peaks in the region of 1300−1730 cm^{-1}. Especially, the two strongest peaks are assigned to be the exocyclic C═C double bond stretching at 1650 cm^{-1} and the C═O stretching of the carbonyl group on the imidazolidinone moiety at 1720 cm^{-1}, respectively.

In Figure 9b, we present the transient infrared absorption spectra of *o*-HBDI recorded at different time delays between the pump pulse (400 nm) and the infrared probe pulses. Clearly, the negative signals of ΔA at 1650 and 1720 cm^{-1}, respectively, originate from the ground-state absorption bleaching upon electronic excitation. The decay time constants of the bleaching signals at 1650 and 1720 cm^{-1} were fit to be 6.7 ± 0.3 and 6.5 ± 0.3 ps, respectively. Given the relatively low sensitivity in the transient IR measurement, the results are qualitatively consistent with both fluorescence decay (7.8 ps) and transient UV/vis absorption (7.6 ps) in CH_3CN. On the other hand, several positive ΔA signals also appear in the frequency region from

dx.doi.org/10.1021/ja107945m |*J. Am. Chem. Soc.* 2011, 133, 2932–2943

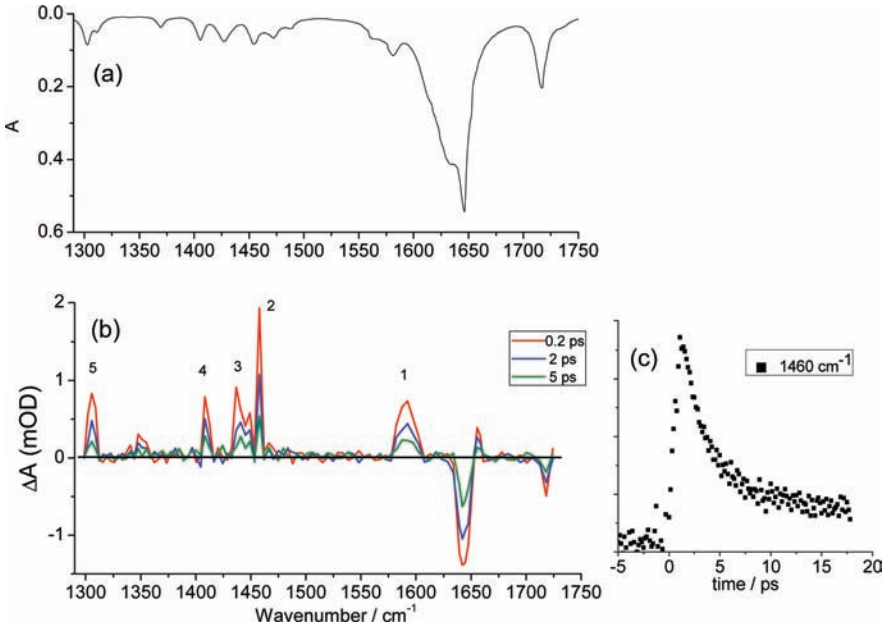

Figure 9. (a) The ground-state FT-IR spectrum of *o*-HBDI in CD_3CN. (b) Transient infrared spectra of *o*-HBDI in CD_3CN after excitation at 400 nm. (c) Transient signal decay monitored at 1460 cm^{-1}.

Table 2. Calculated Infrared Absorption Bands of *o*-HBDI at Cis-Normal Form Ground State (S_0), Cis-Tautomer Form Excited-State (S_1), and Trans-Tautomer Form Ground State (S_0) in CH_3CN

cis-normal form (S_0)		cis-tautomer form (S_1)		trans-tautomer form (S_0)	
cm^{-1}	assignment	cm^{-1}	assignment	cm^{-1}	assignment
1331	δ(O−H) + δ(Ph)	119.72	δ(ex:C═C)	1308	δ(N−H)
1446	ρ(C:CH_3) + ρ(N:CH_3)	248.97	δ(ex:C═C)	1352	δ(N−H) + δ(ex:C−H)
1483	δ(C:CH_3) + ρ(N:CH_3)	1374	δ(N:CH_3) + δ(ex:C−C)	1411	δ(Ph) + δ(N−H) + ρ(C:CH_3)
1514	δ(C:CH_3) + ρ(N:CH_3)	1400	δ(N−H)	1488	δ(C:CH_3)
	+ δ(O−H) + δ(Ph)	1584	ρ(C:CH_3) + ρ(N:CH_3)	1533	δ(Ph) + δ(N−H) + υ(ex:C−C)
1611	δ(O−H) + δ(Ph)	1660	δ(Ph)	1593	υ(ex:C−C) + δ(C:CH_3)
1634	υ(C═N) + υ(ex:C═C)	1714	υ(Ph:C═O) + υ(C═N)		+ υ(C═N) + δ(Ph)
1666	δ(O−H) + δ(Ph)			1710	υ(Ph:C═O)
1689	υ(ex:C═C)			1786	υ(Im:C═O)
1798	υ(Im:C═O)				

[a] υ = stretching mode, δ = in-plane deformation mode, ρ = out-of-plane bending mode, ex = exocyclic C−C═C bonds, Ph = phenol ring, Im = imidazole moiety.

1300 to 1700 cm^{-1}, which are marked by peaks 1−5. The positive signals represent the vibrational spectrum of the growing new species. As shown in Figure 9b, the relaxation dynamics of transient IR absorption bands at 1 (1600 cm^{-1}), 4 (1420 cm^{-1}), and 5 (1310 cm^{-1}) can be described by a single exponential decay, which was fit to be 6.2, 6.5, and 6.3 ps, respectively. Within experimental error, peaks 1, 4, and 5 undergo similar decay dynamics, which also correlate well with fluorescence lifetime in CH_3CN. Thus, their assignment to the vibrational spectra of proton-transfer tautomer at the S_1 state is unambiguous. Interestingly, as shown in Figure 9c, the decay kinetics of peaks 2 (1460 cm^{-1}) and 3 (1450 cm^{-1}) could only be fit by a double exponential, consisting of a fast decay of ∼6.8 ps and a much longer component of ≫30 ps that could not be resolved in our current femtosecond IR setup. The much longer transient IR specie seems to correlate with the long-lived ∼580 nm absorption band in the transient absorption measurement (vide supra). Gathering all kinetic and structural information across from steady state to femtosecond regime, we then developed a comprehensive discussion of *o*-HBDI on the mechanisms of an overall proton transfer cycle, the conclusion of which can thus be compared with *p*-HBDI and/or wild type GFP.

4. DISCUSSION

4.1. Mechanism of ESIPT. The combination of the steady-state data and dynamics for both *o*-HBDI and *o*-MBDI unambiguously confirms the occurrence of ESIPT in *o*-HBDI. This is in sharp contrast to the GFP free *p*-HBDI core, for which the proton transfer in the excited state is prohibited.[5,7,8] Instead, *p*-HBDI, which possesses C═C−C dangling covalent bonds within the π conjugation system, undergoes cis−trans-isomerization

dx.doi.org/10.1021/ja107945m |*J. Am. Chem. Soc.* 2011, 133, 2932–2943

in the excited state, similar to those classes of e.g. *cis*−*trans*-stilbenes.[10] Amid cis−trans-isomerization, the excited-state potential energy surface (PES) would closely approach or even intersect with that of the ground state, resulting in a rapid internal conversion. For *p*-HBDI, the isomerization barrier is proposed to be rather small (<1 kcal/mol) in solution at room temperature,[12] as evidenced by the excited-state decay times being as short as a few picoseconds in solution.[7] In protic solvents, the fast isomerization rate is still prevailing over the rate of the proton transfer, which requires incorporation of a diffusive type of solvent reorganization to form a proton relay, namely, a precursor to execute the proton transfer. Such a specific hydrogen-bonding relay exists in wild-type GFP.[1,3,4] For *o*-HBDI, the formation of a seven-membered-ring intramolecular hydrogen bond strongly induces the interaction between the reactant (normal form) and the product (proton transfer tautomer) along the reaction PES. Such a coupling matrix is generally large if the hydrogen bond is strong,[29] giving adiabatic or even barrierless types of PES along the reaction coordinate. Even if the barrier is non-negligible, the proton transfer may take place essentially in a coherent motion, i.e., a ballistic type of proton transfer through the modulation of the barrier by the skeletal vibrations associated with the hydrogen-bonding distance/angle. In either case, the rate of ESIPT is expected to be ultrafast, with the reaction roughly half of the vibrational period of the associated vibrational mode. For *o*-HBDI, this viewpoint is evidenced by the instantaneous rise of the tautomer emission at 600 nm, even though the resolution of the time-resolved fluorescence apparatus is better than 40 fs. In fact, upon the excitation of *o*-HBDI coherently using an ultrashort pulse (25 fs), vibrational oscillation (beating) with frequencies of 115 and 236 cm^{-1} has been resolved in this study. Vibrational analyses of *o*-HBDI in the proton-transfer tautomer form ascribe the 115and 236 cm^{-1} (see above) to the in-plane skeletal modes of 119 and 248 cm^{-1}, respectively, of the proton-transfer tautomer in the lowest lying singlet excited state [obtained by CIS/6-31g(d)]. In fact, these are the two lowest frequency in-plane modes, which modulate the hydrogen-bonding distance. This molecular skeletal deformation involving the variation of hydrogen-bonding distance/angle (Scheme 2), which is then coupled into the ESIPT reaction, is reminiscent of specific oscillations resolved from several ESIPT systems possessing strong intramolecular hydrogen bonds.[18,20,27] Since the ESIPT reaction time is shorter than the period of these vibrations, ESIPT acts as the impulsive excitation to the tautomer to launch the wave packet motion in the tautomer potential surfaces for the vibrational modes, which show large displacement between the reactant and the tautomer.

Followed by ultrafast ESIPT and intramolecular vibrational redistribution (IVR, $\ll$ 1 ps), due to the exergonic reaction thermodynamics, dense and vibrationally hot states should be initially prepared, which then undergo vibrational relaxation via the solvent deactivation. The time constant of vibrational relaxation depends on the zero-point energy difference between the initially prepared states and the lowest lying excited singlet state S_1' (prime sign denotes the proton-transfer tautomer). In a computational approach [TD-DFT/B3LYP/6-31G(d)], the zero-point energy difference between S_1 of the normal form and S_1' is calculated to be ~7 kcal/mol (~2400 cm^{-1}) for *o*-HBDI. Since the pump pulse in current time-resolved measurements was tuned to 400 nm, which is near the onset of S_0 ($v = 0$) → S_1 ($v' = 0$) transition (see Figure 1), an energy gap of 7 kcal/mol is a reasonable guess for the solvent deactivation. For a

Scheme 2. In-Plane Skeletal Deformation Modes of 119.72 (upper) and 248.97 (lower) cm^{-1}, Obtained by CIS/6-31g(d) (see the text for details)

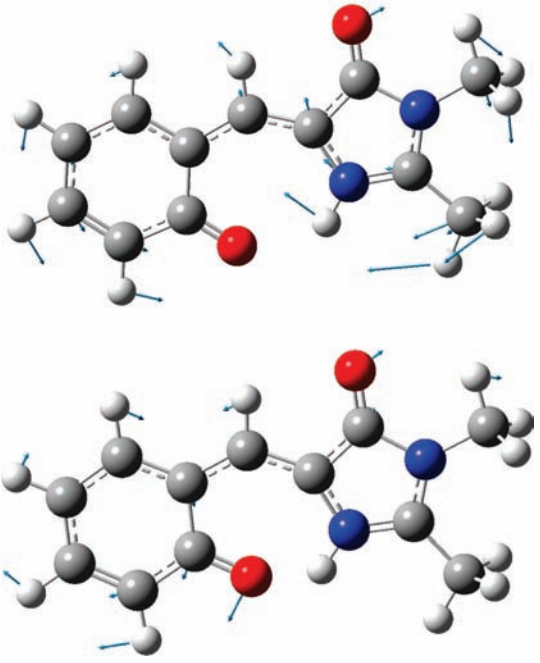

polyatomic molecule, an empirical rule has been drawn that the vibrational relaxation spends about 1 ps for a ~2000 cm^{-1} gap in ordinary organic solvents.[30] Thus, the fast decay component of ~1.0−1.5 ps for *o*-HBDI tautomer emission in various solvents may reasonably be attributed to the time constant of the vibrational relaxation. For the highly exergonic type proton transfer, energy dissipation incorporating IVR, vibrational relaxation, or even internal conversion from the initially prepared highly vibronic state in the early relaxation dynamics is not uncommon and has been reported in several other ESIPT molecules.[18,27]

The fluorescence population decay of 7.8 ps in CH_3CN fits well with the decay (7.2 ps) of the 530 nm transient absorption band; thus, the assignment of 530 nm transient to $S_1'-S_n'$ absorption is unambiguous. Note that the <1.5 ps early vibrational relaxation dynamics observed in the fluorescence upconversion cannot be resolved in the transient absorption measurement, perhaps due to the much broader absorption spectral feature. Accompanied by the 530 nm decay, the growth of a transient absorption band maximized at 580 nm is obvious (Figure 4). Such a precursor−successor type of relationship indicates the growth of another transient species amid excited-state relaxation. Because the fluorescence upconversion measurement did not see any emission with a rise component of 6−8 ps, the new species exhibiting 580 nm transient absorption is more likely to be in the electronic ground state. An additional note is that this 580 nm band, in terms of spectral position and feature, reveals a mirror image with respect to the 602 nm tautomer emission of *o*-HBDI in CH_3CN (Figure 1). From the viewpoint of molecular structure, the proton-transfer tautomer of *o*-HBDI also possesses dangling covalent bonds within the π conjugation system. It is thus reasonable to propose that after ESIPT, the *cis*-*o*-HBDI tautomer may further undergo cis−trans-isomerization, forming a trans-proton transfer tautomer (Scheme 3a,b) in the

Scheme 3. Proposed (a) One-Bond-Flip, (b) Hula-Twist Isomerization Mechanism of *o*-HBDI, and Hula-Twist and One-Bond-Flip Isomerization of (c) Neutral and (d) Zwitterionic *p*-HBDI, respectively, in Solutions

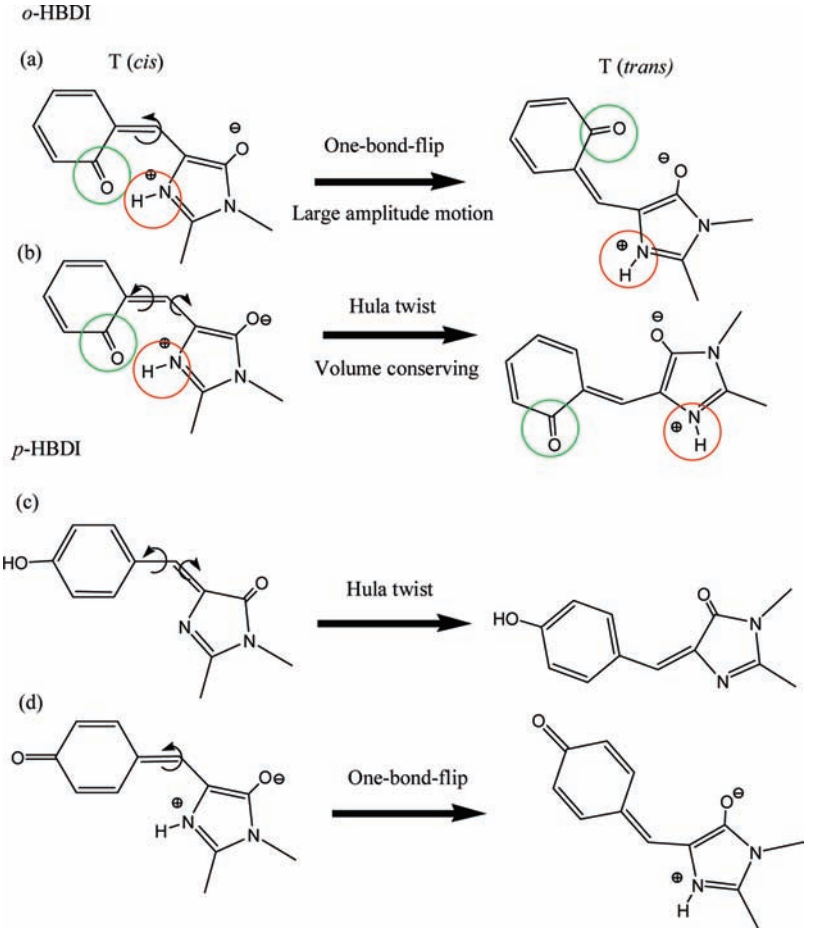

ground state. Supported by the nanosecond transient absorption data, this ground-state transient species is long-lived, having a lifetime of 7.7 μs (vide supra).

As for the mechanism of cis−trans-isomerization, the study of GFP core chromophore, i.e. *p*-HBDI, may serve as a paradigm. In theory, the excited-state isomerization pathway of *p*-HBDI may result from either a one-bond flip around the C═C double bond or the hula-twisted mechanism. The former is induced by rotation of the bridging exocyclic C═C bond, which requires large amplitude motion and is strongly dependent on the solvent viscosity, while the latter involves concerted rotation about the two bridging bonds (Scheme 3c) and thus is more or less independent of solvent viscosity. The relevant data collected so far show the solvent-viscosity-insensitive fluorescence lifetime of *p*-HBDI.[7] The result leads to a volume-conserving isomerization process; in other words, the isomerization of *p*-HBDI is keen to the so-called "hula-twisted" type of isomerization mechanism,[7,12,13] although such a type of mechanism contradicts the results of a recent quantum chemical calculation.[12] Note that similar isomerization has also been observed in other meta isomers of GFP core chromophore, namely, *m*-HBDI analogues.[8] In stark contrast to both *p*-HBDI and *m*-HBDI, as shown in Figure 2 and Table 1, the fluorescence decay of *o*-HBDI in various solvents reveals strong solvent-viscosity dependence, i.e., 7.8 ps in low viscous CH_3CN ($\eta \sim 0.34$ cP), which then elongates to as long as 70.9 ps in viscous solvent such as 1-octadecene ($\eta \sim 3.58$ cP). The enhancement of fluorescence lifetime and hence quantum yield for *o*-HBDI upon increasing solvent viscosity implicitly implies the requirement of large volume change during cis−trans-isomerization. Accordingly, as depicted in Scheme 3, a one-bond flip should be a more favorable isomerization pathway for the proton-transfer tautomer *o*-HBDI .

The great difference in isomerization pathway between *p*-HBDI (neutral and/or anionic form) and *o*-HBDI (zwitterionic form) is of fundamental interest. Recent quantum chemical calculations[12] on the isomerization of zwitterionic species, i.e., the proton transfer tautomer, of *p*-HBDI (see Scheme 3d), indicate that the hula twist of the zwitterionic tautomer structure of *p*-HBDI is energetically unfavorable by 28 kcal/mol en route to the transient state (90° in torsion angle) along the isomerization coordinate. Conversely, a one-bond flip along the C4−C5 bond (see Schemes 1 and 3d for notation) leads to a close approach between excited and ground state PES, which results in an exothermic reaction of 24 kcal/mol toward the 90° torsion angle.[12] Owing to a similar zwitterionic structure, the favorable one-bond-flip pathway for the *o*-HBDI proton-transfer tautomer, concluded from the experimental results, may thus be justified.

Another key issue is the observation of the long-lived trans-proton transfer tautomer in polar solvent such as toluene, tetrahydrofuran, and acetonitrile, but not in nonpolar solvents such as cyclohexane (see section 3.2). Evidently, solvent polarity plays an important role in modifying the cis−trans-isomerization

Scheme 4. Proposed ESIPT and Ground State Reverse Proton Transfer Mechanism of *o*-HBDI in CH_3CN

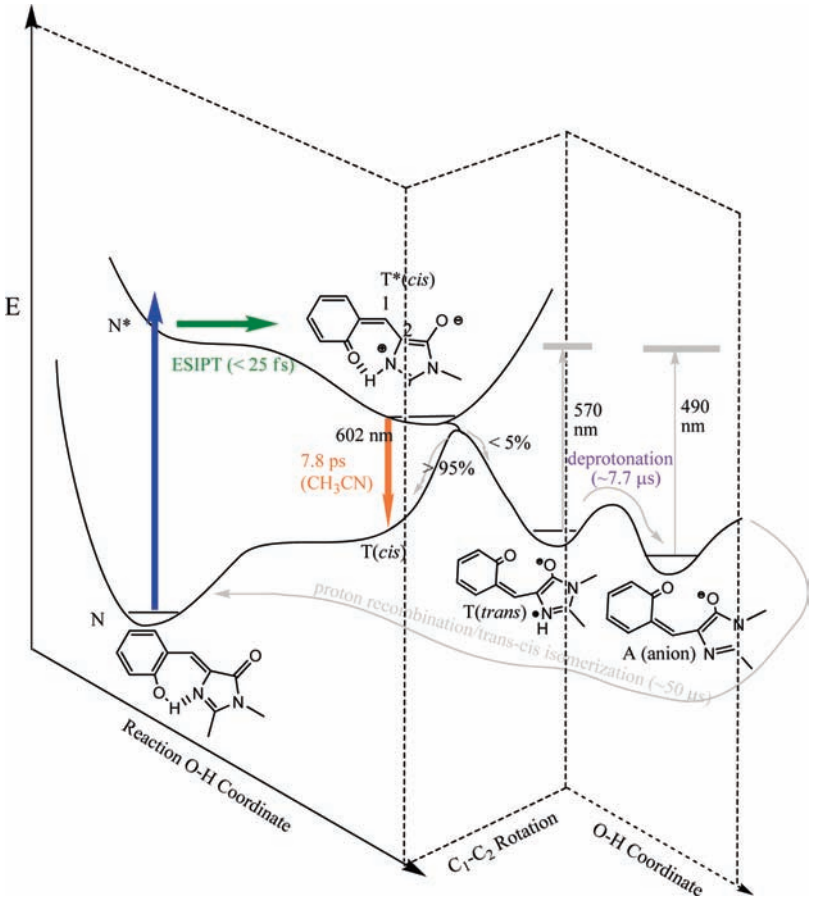

dynamics.[31] Due to the zwitterionic character, rotation of the cisproton transfer tautomer, as shown in Scheme 3, is subject to significant changes in dipolar vector, especially from the viewpoint of dipole orientation during rotation. As a result, equilibrium polarizations between cis- and trans-forms should be far separated along the solvent coordinate.[29] Since the large dipole change in solution is normally coupled to solvent polarization effects, one would expect relative energetics between cis- and trans-forms and the energy barrier to be strongly solvent-polarity-dependent. In nonpolar solvents such as cyclohexane, the lack of polar-charge stabilization energy leads to a high barrier along the cis−trans-isomerization coordinate, such that the rate of cis−trans-isomerization cannot compete with other fast deactivation processes in the case of *o*-HBDI.

Perhaps a direct support of ESIPT as well as the associated cis−trans-isomerization for *o*-HBDI may be provided via the structural analyses, for which UV pump/mid-IR probe time-resolved measurement resolves several transient IR signals (see peaks 1, 4, and 5 in Figure 9). In attempts to resolve these peaks, we also performed the geometry optimization of the cis-tautomer in the S_1' state and then obtained the corresponding vibrational assignments (see Table 2). Incorporating a solvation (CH_3CN) model, the geometry optimization of ground-state trans-tautomer reveals strong IR signals in the region of 1400−1450 cm^{-1}, which are assigned to motions associated with the in-plane deformation of the phenyl ring. However, a definitive match between experimental and computational results seems impossible. This may be in part due to the fact that the current theoretical level is not sophisticated enough to describe the proton-transfer tautomer geometry in the excited state. Nevertheless, the appearance of new, distinct IR peaks (Figure 9b) evidences significant structural changes upon ESIPT. It is also noteworthy that peaks 2 (1460 cm^{-1}) and 3 (1450 cm^{-1}) could only be fit by double exponential decay kinetics, consisting of a fast decay of ~6.8 ps and a much longer component of ≫30 ps. The former can reasonably be assigned to the overlapping IR peaks of the cis-tautomer in the S_1 state, while the latter, the much longer transient IR peaks, are most plausibly attributed to the trans-tautomer in the ground state. This assignment is in accordance with that concluded in the transient absorption measurement. We have also performed careful data analyses by plotting peak 2 and 3 spectra appearing at two extreme time domains, i.e., 1 and 30 ps, in an attempt to resolve the associated time-dependent IR peaks. Unfortunately, differentiation still cannot be made plausibly due to the limited spectral resolution.

On the basis of the above results and discussion, triggered by ESIPT, an overall proton transfer cycle of *o*-HBDI in CH_3CN can thus be depicted in Scheme 4. Upon electronic excitation, *o*-HBDI undergoes an ultrafast, perhaps barrierless, ESIPT (<25 fs), forming a proton-transfer cis-tautomer at the S'_1 state. Subsequently, along the rotation of the exocyclic C═C bond, the associated excited-state PES seems to closely couple with the ground-state PES, resulting in a fast internal conversion process. As indicated by the >95% recovery of the stimulated emission at the early 130 ps time regime, we estimate that a small

dx.doi.org/10.1021/ja107945m |*J. Am. Chem. Soc.* 2011, 133, 2932–2943

portion (<5%) of the cis-tautomer isomerizes to a long-lived trans-tautomer.

Interestingly, in a polar solvent such as CH_3CN, as indicated by the growth of λ_{abs} = 500 nm accompanied by the decay of $\sim\lambda_{abs}$ = 575 nm trans-proton transfer tautomer (see Figures 7 and 8), the trans-tautomer then relaxes to another species, rather than back to the cis-proton transfer tautomer. Upon excitation of the 500 nm band, TSLIF gives rise to an emission maximized at 580 nm. Due to its similarity with the absorption (~480 nm) and emission (~580 nm) spectra of the deprotonated *cis-o*-HBDI (see Figure 1), we propose that the trans-proton transfer tautomer then undergoes deprotonation to the surrounding solvent (CH_3CN) due to its lack of an intramolecular hydrogen bond (see Scheme 4), though direct structural evidence is still pending proof. Supplementary support of this viewpoint is that this 500 nm transient is not observed in a less polar or nonpolar solvent such as toluene or cyclohexane. The anionic species then undergoes reverse proton transfer (protonation), together with trans−cis-isomerization, en route to the original ground-state *cis-o*-HBDI. These processes are expected to be rather slow, such that further exploration is not pursued.

5. CONCLUSION

In sum, comprehensive ultrafast time-resolved fluorescence, UV/vis transient absorption, and UV/mid-IR time-resolved spectroscopy and dynamics of *o*-HBDI in solution have been carried out. The *o*-HBDI proton-transfer tautomer emission, resolved by fluorescence upconversion with a time resolution of ~25 fs, is comprised of an instantaneous rise to a few hundred femtosecond oscillation in the early relaxation stage. Frequency analysis deduces two low-frequency vibrations at 115 and 236 cm^{-1}, corresponding to skeletal deformation motions associated with the hydrogen bonds. This cis-proton transfer tautomer at the S'_1 state then undergoes mainly radiationless deactivation, possibly induced by the exocyclic C=C bond rotation. Approximately 5% of cis-proton transfer tautomer undergoes full cis−trans-isomerization to a long-lived, ground-state trans-tautomer, which is then deprotonated, forming an anion species in the polar solvent such as CH_3CN. According to the strong solvent-viscosity-dependent relaxation dynamics, the cis−trans-isomerization is in favor of the one-bond flip of the exocyclic C=C bond with large amplitude motion. Structural variations upon ESIPT and cis−trans-isomerization are also qualitatively identified by transient IR spectra. The results provide fair comparison of *o*-HBDI and GFP core chromophore *p*-HBDI. The key difference lies in that *o*-HBDI possesses an intrinsic seven-membered-ring intramolecular hydrogen bond, such that ultrafast, barrierless-like ESIPT takes place, followed by the isomerization and deprotonation (in CH_3CN) process. Conversely, ESPT is prohibited in *p*-HBDI; instead, cis−trans-isomerization takes place in the Franck−Condon excited-state. The zwitterionic (*o*-HBDI) cis-tautomer versus neutral (*p*-HBDI) normal form in nature results in the difference in isomerization, i.e., the one-bond-flip (*o*-HBDI) versus the hula-twist (*p*-HBDI) mechanism. In the ground state, the lifetime of trans-tautomer is determined to be ~7.7 μs, which is attributed to a deprotonation process to form the anion specie. Finally, the anion specie undergoes a ~50 μs proton recombination together with reverse isomerization to recover the ground state normal form, generating a reversible ESIPT → cis−trans-isomerization → deprotonation → reverse ground-state protonation cycle that is distinctly different from *p*-HBDI, *m*-HBDI as well as the wild-type GFP.

AUTHOR INFORMATION

Corresponding Author
chop@ntu.edu.tw; thjoo@postech.ac.kr

ACKNOWLEDGMENT

P.-T.C. and T.J. thank the National Science Council, Taiwan, and the National Research Foundation (2010-0001634) of Korea, respectively, for financial support. We are also grateful to the National Center for High-Performance Computing of Taiwan, for allowing us generous amounts of computing time.

REFERENCES

(1) (a) Chalfie, M.; Tu, Y.; Euskirchen, G.; Ward, W. W.; Prasher, D. C. *Science* **1994**, *263*, 802. (b) Lippincott-Schwartz., J.; Patterson, G. H. *Science* **2003**, *300*, 87. (c) Ormo, M.; Cubitt, A. B.; Kallio, K.; Gross, L. A.; Tsien, R. Y.; Remington, S. J. *Science* **1996**, *273*, 1392. (d) Zimmer, M. *Chem. Rev.* **2002**, *102*, 759. (e) Tsien, R. Y. *Annu. Rev. Biochem.* **1998**, *67*, 509.(f) Sullivan, K. F.; Kay, S. A. *Green Fluorescent Proteins*; Academic Press: San Diego, CA, 1999.

(2) Brejc, K.; Sixma, T. K.; Kitts, P. A.; Kain, S. R.; Tsien, R. Y.; Ormo, M.; Remington, S. J. *Proc. Natl. Acad. Sci. U.S.A.* **1997**, *94*, 2306.

(3) (a) Chattoraj, M.; King, B. A.; Bublitz, G. U.; Boxer, S. G. *Proc. Natl. Acad. Sci. U.S.A.* **1996**, *93*, 8362. (b) Agmon, N. *Biophys. J.* **2005**, *88*, 2452. (c) Hosoi, H.; Mizuno, H.; Miyawaki, A.; Tahara, T. *J. Phys. Chem. B* **2006**, *110*, 22853.

(4) (a) Stoner-Ma, D.; Jaye, A. A.; Matousek, P.; Towrie, M.; Meech, S. R.; Tonge, P. J. *J. Am. Chem. Soc.* **2005**, *127*, 2864. (b) Stoner-Ma, D.; Melief, E. H.; Nappa, J.; Ronayne, K. L.; Tonge, P. J.; Meech, S. R. *J. Phys. Chem. B* **2006**, *110*, 22009. (c) Shu, X.; Kallio, K.; Shi, X.; Abbyad, P.; Kanchanawong, P.; Childs, W.; Boxer, S. G.; Remington, S. J. *Biochemistry* **2007**, *46*, 12005. (d) Su, X.; Abbyad, P.; Shu, X.; Kallio, K.; Kanchanawong, P.; Childs, W.; Remington, S. J.; Boxer, S. G. *Biochemistry* **2007**, *46*, 12014. (e) Leiderman, P.; Genosar, L.; Huppert, D.; Shu, X.; Remington, S. J.; Solntsev, K. M.; Tolbert, L. M. *Biochemistry* **2007**, *46*, 12026. (f) Stoner-Ma, D.; Jaye, A. A.; Ronayne, K. L.; Nappa, J.; Meech, S. R.; Tonge, P. J. *J. Am. Chem. Soc.* **2008**, *130*, 1227. (g) Kondo, M.; Heisler, I. A.; Stoner-Ma, D.; Tonge, P. J.; Meech, S. R. *J. Am. Chem. Soc.* **2010**, *132*, 1452.

(5) (a) Niwa, H.; Inouye, S.; Hirano, T.; Matsuno, T.; Kojima, S.; Kubota, M.; Ohashi, M.; Tsuji, F. I. *Proc. Natl. Acad. Sci. U.S.A.* **1996**, *93*, 13617. (b) Dong, J.; Solntsev, K. M.; Tolbert, L. M. *J. Am. Chem. Soc.* **2006**, *128*, 12038. (c) Yang, J. S.; Huang, G. J.; Liu, Y. H.; Peng, S. M. *Chem. Commun.* **2008**, 1344.

(6) He, X.; Bell, A. F.; Tonge, P. J. *Org. Lett.* **2002**, *4*, 1523.

(7) (a) Mandal, D.; Tahara, T.; Webber, N. M.; Meech, S. R. *Chem. Phys. Lett.* **2002**, *358*, 495. (b) Litvinenko, K. L.; Webber, N. M.; Meech, S. R. *J. Phys. Chem. A* **2003**, *107*, 2616. (c) Mandal, D.; Tahara, T.; Meech, S. R. *J. Phys. Chem. B* **2004**, *108*, 1102.

(8) (a) Dong, J.; Solntsev., K. M.; Poizat, O.; Tolbert, L. M. *J. Am. Chem. Soc.* **2007**, *129*, 10084. (b) Solntsev, K. M.; Poizat, O.; Dong, J.; Rehault, J.; Lou, Y.; Burda, C.; Tolbert, L. M. *J. Phys. Chem. B* **2008**, *112*, 2700.

(9) Usman, A.; Mohammed, O. F.; Nibbering, E. T. J.; Dong, J.; Solntsev, K. M.; Tolbert, L. M. *J. Am. Chem. Soc.* **2005**, *127*, 11214.

(10) (a) Todd, D. C.; Fleming, G. R. *J. Chem. Phys.* **1993**, *98*, 269. (b) Saltiel, J.; Waller, A. S.; Sears, D. F., Jr. *J. Am. Chem. Soc.* **1993**, *115*, 2453. (c) Ishii, K.; Takeuchi, S.; Tahara, T. *Chem. Phys. Lett.* **2004**, *398*, 400.

(11) (a) Stavrov, S. S.; Solntsev, K. M.; Tolbert, L. M.; Huppert, D. *J. Am. Chem. Soc.* **2006**, *128*, 1540. (b) Gepshtein, R.; Huppert, D.; Agmon, N. *J. Phys. Chem. B* **2006**, *110*, 4434.

(12) Weber, W.; Helms, V.; McCammon, J. A.; Langhoff, P. W. *Proc. Natl. Acad. Sci. U.S.A.* **1999**, *96*, 6177.
(13) Liu, R. S. H. *Acc. Chem. Res.* **2001**, *34*, 555.
(14) Dong, J.; Abulwerdi, F.; Baldridge, A.; Kowalik, J.; Solntsev, K. M.; Tolbert, L. M. *J. Am. Chem. Soc.* **2008**, *130*, 14096.
(15) Fang, C.; Frontiera, R. R.; Tran, R.; Mathies, R. A. *Nature* **2009**, *462*, 200.
(16) Chen, K. Y.; Cheng, Y. M.; Lai, C. H.; Hsu, C. C.; Ho, M. L.; Lee, G. H.; Chou, P. T. *J. Am. Chem. Soc.* **2007**, *129*, 4534.
(17) Chou, P. T.; Chen, Y. C.; Yu, W. S.; Chou, Y. H.; Wei, C. Y.; Cheng, Y. M. *J. Phys. Chem. A* **2001**, *105*, 1731.
(18) (a) Rhee, H.; Joo, T. *Opt. Lett.* **2005**, *30*, 96. (b) Kim, C. H.; Joo, T. *Opt. Express* **2008**, *16*, 20742. (c) Kim, C. H.; Joo, T. *Phys. Chem. Chem. Phys.* **2009**, *11*, 10266.
(19) Duan, H. S.; Chou, P. T.; Hsu, C. C.; Hung, J. Y.; Chi, Y. *Inorg. Chem.* **2009**, *48*, 6501.
(20) Rini, M.; Kummrow, A.; Dreyer, J.; Nibbering, T. J.; Elsaesser, T. *Faraday Dicsuss.* **2002**, *122*, 27.
(21) Brewer, W. E.; Studer, S. L.; Standiford, M.; Chou, P. T. *J. Phys. Chem.* **1989**, *93*, 6088.
(22) (a) Lee, C.; Yang, W.; Parr, R. G. *Phys. Rev. B* **1988**, *37*, 785. (b) Becke, A. D. *J. Chem. Phys.* **1993**, *98*, 5648.
(23) Foresman, J. B.; Head-Gordon, M.; Pople, J. A.; Frisch, M. J. *J. Phys. Chem.* **1992**, *96*, 135.
(24) Hariharan, P. C.; Pople, J. A. *Mol. Phys.* **1974**, *27*, 209.
(25) Cancès, M. T.; Mennucci, B.; Tomasi, J. *J. Chem. Phys.* **1997**, *107*, 3032.
(26) *Gaussian 03, revision C.02*; Gaussian, Inc., Wallingford, CT, 2004.
(27) Takeuchi, S.; Tahara, T. *J. Phys. Chem. A* **2005**, *109*, 10199.
(28) Sanz, M.; Douhal, A. *Chem. Phys. Lett.* **2005**, *401*, 435.
(29) Hsieh, C. C.; Jiang, C. M.; Chou, P. T. *Acc. Chem. Res.* **2010**, *43*, 1364.
(30) Elsaesser, T.; Kaiser, W. *Annu. Rev. Phys. Chem.* **1991**, *42*, 83.
(31) (a) Chou, P. T.; Huang, C. H.; Pu, S. C.; Cheng, Y. M.; Liu, Y. H.; Wang, Y.; Chen, C. T. *J. Phys. Chem. A* **2004**, *108*, 6452. (b) Chou, P. T.; Pu, S. C.; Cheng, Y. M.; Yu, W. S.; Yu, Y. C.; Hung, F. T.; Hu, W. P. *J. Phys. Chem. A* **2005**, *109*, 3777. (c) Hsieh, C. C.; Chen, K. Y.; Hsieh, W. T.; Lai, C. H.; Shen, J. Y.; Jiang, C. M.; Duan, H. S.; Chou, P. T. *ChemPhysChem* **2008**, *9*, 2221. (d) Hsieh, C. C.; Cheng, Y. M.; Hsu, C. J.; Chen, K. Y.; Chou, P. T. *J. Phys. Chem. A* **2008**, *112*, 8323.